Tight-binding potentials for transition metals and alloys

Fabrizio Cleri and Vittorio Rosato
Ente per le Nuove Tecnologie, L'Energìa e L'Ambiente, Divisione Scienza dei Materiali, Centro Ricerche Energetiche della Casaccia, Casella Postale 2400, I-00100 Roma A.D., Italy
(Received 23 November 1992; revised manuscript received 11 February 1993)

The parameters of many-body potentials for fcc and hcp transition metals, based on the second-moment approximation of a tight-binding Hamiltonian, have been systematically evaluated. The potential scheme, cast in analytical form, allows us to reproduce correctly the thermal behavior of transition metals making use of a small set of adjustable parameters. The large cutoff, which extends the range of the interactions up to the fifth-neighbor distance, ensures good quantitative agreement with the experimental data up to temperatures close to the melting point. The ability of the potentials to describe real systems has been checked by calculating point-defect properties, lattice dynamics, and finite-temperature behavior, and by comparing the results with other potential schemes. Application of this scheme to bcc transition metals has proved unsuccessful. Examples of derivation of many-body potentials for a few transition-metal alloys with cubic structure are also reported.

I. INTRODUCTION

It is widely recognized that empirical many-body potentials can reproduce with good accuracy the thermodynamic and structural properties of most transition metals.[1–3] In the last years, these potentials have been extensively used to analyze a variety of problems in materials science by molecular-dynamics (MD) computer simulations. The use of empirical potentials is, while waiting for appropriate extensions of the more general Car-Parrinello technique,[4] the only practical way to approach the simulation of point or extended defects (vacancies, grain boundaries, or dislocations), interfaces, and surface properties for transition metals and intermetallic alloys.[5–11]

The main advantage of a many-body treatment over the conceptually and practically simpler pair-potential description is the ability to better reproduce some basic features of metallic systems. First of all, the so-called Cauchy discrepancy of the elastic constants, namely, the experimental evidence that for most cubic crystals $C_{12} \neq C_{44}$, which cannot be accounted for by pair potentials. Another serious drawback of the use of pair potentials is represented by the incorrect estimates of the vacancy formation energies, whose values result very nearly equal to the cohesive energies, whereas the experimental results indicate that they range around $\frac{1}{3}$ of the cohesive energy. Furthermore, stacking fault energies, surface structure, and relaxation properties cannot be properly accounted for by means of pair potentials. A many-body potential scheme overcomes these difficulties by including, even at a phenomenological level, the essential band character of the metallic bond. A relatively simple scheme for relating the atomic and electronic structure, without resorting to the complex treatment of first-principles calculations, is the tight-binding (TB) method[12–14] in which the ion-ion interaction is described as made up of an effective band term plus a short-range repulsive pair potential. The second-moment approximation of the tight-binding scheme (TB-SMA) as proposed by Tomanek, Aligia, and Balseiro[15] is based on a small set of adjustable parameters and, at least in principle, is suitable for extension to higher-order approximation through extension to higher moments of the electron density of states (DOS). It was originally introduced with a very short cutoff restricting the interaction to the first-neighbors shell. Indeed, it has been shown by several authors[16,17] that extensions of the scheme up to including a sufficient number of neighbors can considerably improve the quality of the results. In particular, Willaime and Massobrio[17] have reproduced the high-temperature hcp-bcc transition in Zr, with a TB potential of the type discussed in the following, extended to include fifth neighbors.

The aim of the present work is to fully exploit the capabilities of the TB-SMA potential scheme by evaluating the set of adjustable parameters of the model for a large number of transition metals and some alloys, and to show its ability in reproducing experimental finite-temperature results. The improved agreement is obtained by including a suitable number of interacting atoms per lattice site within the cutoff range of the potential (typically up to fifth neighbors), so as to produce a class of potentials to be used in large-scale MD computer simulations of pure transition metals and of their alloys.

The paper is organized as follows: in Sec. II, the fundamentals of the TB-SMA model, its relation with the tight-binding scheme, and with the other commonly used many-body models are recalled; in Sec. III, the TB-SMA potential model is developed for fcc, hcp, and bcc structures of pure metals, and for fcc-based structures of intermetallic alloys; in Sec. IV, the obtained potentials are tested against some static and finite-temperature experimental quantities, also including phonon properties; finally, in Sec. V, conclusions and comments are drawn.

II. THE TIGHT-BINDING SECOND-MOMENT MODEL

It is well known that the cohesive properties of transition metals and their alloys originate from the large d-band density of states. Several thermodynamic and

0163-1829/93/48(1)/22(12)/$06.00

structural quantities have been shown to be insensitive to the details of the electron DOS, $n(E)$,[18] being mainly related to its average value and effective width.

The description of the electron DOS in terms of its moments is a natural tool to relate the electronic structure to the lattice topology, since moments are obtained by calculating products of matrix elements of the electron Hamiltonian associated with closed paths of definite length. Each moment μ_k can then be interpreted as the contribution to the DOS coming from all possible closed electron paths of k steps. In particular, the first moment μ_1, related to the band center energy, fixes the energy scale and can be set to zero in pure systems. The experimental binding energies of transition metals appear, in turn, to be roughly proportional to the average width of the DOS, described by $\sqrt{\mu_2}$.[19] A basic result of the TB model for transition metals is that, under the constraint of local charge neutrality, an analytic expression for the first few moments can be written if the sums are restricted to first neighbors only in fcc or hcp, and to second neighbors in bcc structures. Electron d bands can then be described by a basis of two-center integrals (*hopping* or "overlap" integrals, as the matrix elements describe the overlapping of TB wave functions). The energy eigenvalues of the resulting matrix are classified, according to the magnetic quantum number of the basic orbitals, as $dd\sigma$, $dd\pi$, and $dd\delta$ (the Slater-Koster parameters[20]), and the moments are, accordingly, linear combinations of these integrals. In particular, the second moment of the electron DOS can be written as a sum of squares of hopping integrals

$$\mu_2 = z(dd\sigma^2 + 2dd\pi^2 + 2dd\delta^2) \tag{1}$$

describing those matrix elements in the Hamiltonian with electron paths starting from a given site, jumping to one other and jumping back to the original one, z being the coordination number (self-retracing paths do not appear in the sum). Moments of higher order cannot be expressed in an analytic form, and more complex techniques, like the recursion method,[21] must be applied.

As the hopping integrals are a function only of the radial distance between atoms i and j, the band energy, proportional to the square root of μ_2, can be written for an atom i as[3,15]

$$E_B^i = -\left\{ \sum_j \xi_{\alpha\beta}^2 e^{-2q_{\alpha\beta}(r_{ij}/r_0^{\alpha\beta}-1)} \right\}^{1/2}, \tag{2}$$

where r_{ij} represents the distance between atoms i and j and $r_0^{\alpha\beta}$ is the first-neighbors distance in the $\alpha\beta$ lattice. ξ is an effective hopping integral, and q describes its dependence on the relative interatomic distance. The standard dependence of the Slater-Koster parameters should rather be r^{-4} or r^{-5}, but the exponential form, widely used as well, better accounts for atomic relaxation near impurities and surfaces, as suggested by Tomànek *et al.*[15] Both q and ξ are assumed to depend only on the interacting atomic species α and β.

In order to ensure crystal stability, a repulsive interaction term is needed aside of the bonding contribution of Eq. (2). This is normally assumed to be pairwise and described by a sum of Born-Mayer ion-ion repulsions

$$E_R^i = \sum_j A_{\alpha\beta} e^{-p_{\alpha\beta}(r_{ij}/r_0^{\alpha\beta}-1)} \tag{3}$$

originating from the increase in kinetic energy of conduction electrons constrained within two approaching ions.[18] Thus, the parameter p, still depending on the interacting atomic species only, should be related to the compressibility of the bulk metal. Indeed, this pair term should contain all the energy after the one-electron sums explicitly included in the overlap integrals, i.e., pair electrostatic interaction plus exchange and correlation terms, which, in turn, can only be approximately represented by a pairwise form. Moreover, it has been suggested[22] that the Born-Mayer term should also cumulate the sum over local crystal-field terms that are subtracted in the construction of the hopping integrals.

The total cohesive energy of the system is then

$$E_c = \sum_i (E_R^i + E_B^i) \tag{4}$$

with the band term, quantum mechanical in origin, incorporating a many-body summation.

The form (2) for the band term is generally equivalent to a functional expression of the type $-A\sum_i F(\rho_i)$, with $\rho_i = \sum_j \phi(r_{ij})$ representing a sum over the local electronic charge density ϕ induced at site i from atoms at sites j. In this sense the TB-SMA model is formally analogous, even if originating from a different physical picture, to the "embedded-atom method" (EAM) model by Daw and Baskes,[1] especially in its simplified version introduced by Oh and Johnson[10] in which case the form of the electron density function ϕ is just set to a simple exponential. In more details, Jacobsen, Nørskov, and Puska[23] showed the embedding function $F(\rho)$ to be mainly related, in the case of d-band metals, to the sum of occupied one-electron energies, which are described by the empirical many-body term in the TB-SMA model. This result is even more meaningful, when compared to the derivation of Daw[24] in which the EAM model is only related to local electron-density properties, completely discarding band-structure effects. The ingredients EAM uses are related to ground-state free-atom electron densities, and transposition to bulk systems is done by empirical adjustment of further free parameters, in a way completely similar to TB and Finnis-Sinclair[2] (FS) models.

The analogy of the TB-SMA scheme with the FS treatment appears even more evident. In fact, in the FS model the F functional "is set to a square root in order to mimic the results of the tight-binding model."[2] The differences reside in the analytical form of the local interatomic functions that are casted as polynomials of third and fourth degree in r_{ij} for the binding and pairwise terms, respectively. In particular, this amounts to say that the spatial dependence of the hopping integrals is linear rather than exponential. It is worth noting that all the TB-SMA, EAM of any kind, and FS schemes share the rectangular approximation for the electron DOS, centered at μ_1 and of width $\sqrt{\mu 2}$.

The free parameters A, ξ, p, q, and r_0 of the SMA scheme are fitted to the experimental values of cohesive

TABLE I. Parameters of TB potentials for fcc transition metals and for the two simple metals Al and Pb.

	A (eV)	ξ (eV)	p	q
Ni	0.0376	1.070	16.999	1.189
Cu	0.0855	1.224	10.960	2.278
Rh	0.0629	1.660	18.450	1.867
Pd	0.1746	1.718	10.867	3.742
Ag	0.1028	1.178	10.928	3.139
Ir	0.1156	2.289	16.980	2.691
Pt	0.2975	2.695	10.612	4.004
Au	0.2061	1.790	10.229	4.036
Al	0.1221	1.316	8.612	2.516
Pb	0.0980	0.914	9.576	3.648

energy, lattice parameters (by a constraint on the atomic volume), and independent elastic constants for each pure system and for alloys, in the appropriate crystal structure at $T=0$ K temperature, and by taking the equilibrium conditions into account. The summation over j in Eqs. (2) and (3) is extended up to the fifth neighbors for cubic structures, and up to the ninth neighbors for the hcp structure.

The second-moment approximation is supposed not to be suited, in principle, for noble metals whose cohesive energy, mainly related to *s-d* hybridization, claims for the inclusion of higher moments of the electron DOS. Failure of SMA is also generally expected when the relative fcc-hcp-bcc stability across the transition series is investigated. In fact,[18] for close-packed structures, $\mu_3 \sim \mu_2$ and the fourth moment can be roughly expressed as $\mu_4=\mu_2^2(2-1/z)$; then, the coordination z for close-packed structures being around 12–14, it is clear that μ_4 is not very sensitive to the lattice topology, and one has to include at least μ_5 to clearly distinguish between the different structures.

However, it will be shown in the following that the simple extension of the TB-SMA model to a sufficiently longer range gives in most cases a quite good agreement with experimental anisotropy constants, for both transition and noble metals. These results, together with the similarities between transition and noble metals in the cohesive and surface energies and bulk moduli, empirically support the use of this same model with no need for the introduction of further free parameters.

III. APPLICATIONS

A. Close-packed structure metals

In fcc metals the equilibrium conditions result in only one equation for any of the equivalent [100] directions. Three further relations are obtained equating the second derivative of the cohesive energy Eq. (4) to the three independent elastic constants C_{11}, C_{12}, and C_{44} in Voigt's notation. The first-neighbor distance $r_0=a_0/\sqrt{2}$ is kept fixed at the experimental value of the fcc lattice parameter giving the correct atomic volume $\Omega_0=a_0^3/4$. The resulting sets of potential parameters for all the fcc transition metals and noble metals, plus the two *s,p*-bonded metals Al and Pb, are listed in Table I; the results of the fitting procedure are reported in Table II, together with a comparison to experimental data and to the results from other models, whenever available. Application of the tight-binding model to *sp* metals is done by identifying the many-body summation in Eq. (2) with the volume-

TABLE II. Values of the fitted quantities for fcc metals. First lines contain the calculated values. (a) experimental values: a_0 (Å) and E_c (eV) from Kittel (Ref. 60), elastic constants (Mbar) from Simmons and Wang (Ref. 61); (b) results of this same model, with cutoff limited to first neighbors; (c) third-neighbor EAM model (Ref. 9); (d) long-range FS model (Ref. 7).

	$-E_c$	a_0	C_{11}	C_{12}	C_{44}	$\langle B \rangle$	C'	C/C'
Ni	4.435	3.523	2.57	1.55	1.36	1.89	0.51	2.67
		(a)	2.61	1.51	1.32	1.88	0.55	2.40
		(b)	2.57	1.65	0.93	1.96	0.46	2.00
		(c)	2.33	1.54	1.28	1.80	0.40	3.24
		(d)	2.31	1.78	0.80	1.95	0.27	2.96
Cu	3.544	3.615	1.76	1.25	0.82	1.42	0.26	3.15
		(a)	1.76	1.25	0.82	1.42	0.26	3.15
		(b)	1.82	1.14	0.68	1.37	0.34	2.00
		(c)	1.67	1.24	0.76	1.38	0.22	3.45
		(d)	1.70	1.30	0.58	1.43	0.20	2.90
Rh	5.752	3.803	3.92	2.37	1.99	2.89	0.77	2.58
		(a)	4.22	1.92	1.94	2.69	1.15	1.69
		(b)	3.84	2.20	1.65	2.74	0.83	2.00
		(d)	3.40	2.32	1.43	2.69	0.54	2.65
Pd	3.936	3.887	2.32	1.78	0.73	1.96	0.26	2.81
		(a)	2.34	1.76	0.71	1.95	0.29	2.45
		(b)	2.36	1.66	0.69	1.90	0.34	2.00
		(c)	2.18	1.84	0.65	1.95	0.17	3.82
		(d)	2.48	1.76	0.93	2.00	0.36	2.58
Ag	2.960	4.085	1.32	0.97	0.51	1.08	0.18	2.83
		(a)	1.31	0.97	0.51	1.08	0.17	3.00
		(b)	1.32	0.92	0.40	1.05	0.20	2.00
		(c)	1.29	0.91	0.57	1.04	0.19	3.00
		(d)	1.41	0.96	0.59	1.11	0.23	2.57
Ir	6.928	3.839	5.54	3.45	2.61	4.15	1.04	2.51
		(a)	5.99	2.56	2.69	3.70	1.72	1.56
		(b)	5.05	2.98	2.07	3.68	1.04	2.00
		(d)	4.76	3.11	2.11	3.65	0.83	2.54
Pt	5.853	3.924	3.41	2.73	0.91	2.96	0.34	2.68
		(a)	3.58	2.54	0.77	2.88	0.52	1.48
		(b)	3.29	2.27	1.02	2.61	0.51	2.00
		(c)	3.03	2.73	0.68	2.83	0.15	4.53
		(d)	3.14	2.58	0.74	2.77	0.28	2.64
Au	3.779	4.079	1.87	1.54	0.45	1.65	0.17	2.65
		(a)	1.87	1.55	0.45	1.66	0.16	2.81
		(b)	1.92	1.66	0.39	1.66	0.20	2.00
		(c)	1.83	1.59	0.45	1.67	0.12	3.75
		(d)	1.79	1.47	0.42	1.59	0.16	2.63
Al	3.339	4.050	0.95	0.74	0.37	0.81	0.11	3.36
		(a)	1.07	0.61	0.29	0.76	0.23	1.26
		(d)	0.82	0.72	0.16	0.75	0.05	3.20
Pb	2.043	4.951	0.47	0.37	0.14	0.41	0.05	2.80
		(a)	0.46	0.38	0.14	0.41	0.04	3.40
		(d)	0.50	0.38	0.16	0.42	0.06	2.67

dependent term needed in the usual theory of simple metals.[25]

The agreement reached on the fitted quantities is remarkably good, except for Rh, Ir, and Pt, and Al among the *sp*-bonded metals, for which an average discrepancy of the order of 10% is obtained on the experimental elastic constants. The higher quality of the results is essentially related to the extension to a longer range of the model scheme, by comparison with the issues of this same model when restricted to first neighbors [data labeled (b) in Table II].

The anisotropy ratio C/C' gives an order of magnitude for the variation of the shear response with orientation, and it is generally a difficult quantity to reproduce, due to the fact that, as the fitting uncertainty on C_{44} has opposite sign than that on C', their ratio tends to amplify the errors (however, it could happen that for larger errors made on C_{11} an artificious error compensation occurs). It must be noted that, for interactions restricted to first neighbors only, the TB-SMA model gives the anisotropy constant $C_{44}/C'=2$ whatever the values of p and q, and that the relations $\xi=pE_c/(p-q)\sqrt{z}$ and $A=qE_c/(p-q)z$ hold, so that the model actually reduces to a two-parameter scheme.[3] The present extended model provides accurate results, which rather improve those of the long-range FS model of Sutton and Chen.[7]

In hcp metals the same four-potential free parameters have to be fitted by taking into account two separate equilibrium conditions, in the xy plane and along the z axis, and two further independent elastic constants C_{13} and C_{33}. Moreover, as the system is noncubic, the constant C_{44} must be redefined. The partially noncentral character of the potential in the hcp structure is reflected in the $\beta=c/a$ ratio: for $\beta_0=\sqrt{8/3}$ the hcp crystal is cubic, and coincides with an fcc structure observed along the [111] direction. However, it is to be expected that metallic systems with β strongly different from the ideal value β_0 will be hardly reproduced by our model, which is based on functionals of central interactions. Then, if necessary, β can also be allowed to vary and a constraint on the atomic volume, defined by

$$\Omega_0=\frac{\sqrt{3}}{4}a^3\beta\ , \tag{5}$$

has to be imposed. Table III reports the values of the TB-SMA potential parameters for the hcp metals Ti, Co, Sc, Cd, Zr, and Mg, and in Table IV the results for the quantities in the fitting procedure are compared to the experimental data. These show a reasonable agreement for Co and Mg, which have a value of β very close to β_0, whereas the agreement is progressively worsened as β moves away from the ideal value. Few applications of many-body potentials to hcp metals have been attempted up to now: Oh and Johnson,[10] who computed a potential for Ti, Zr, and Mg with a simplified version of the EAM model, and Willaime and Massobrio, who computed a potential for pure Zr with the TB-SMA scheme[17] and used it in the calculation of the hcp-bcc transition. All these authors used variable values of β, in the impossibility of reaching a good agreement with the experimental data using the experimental β value. The stability of the hcp structure with respect to the cubic fcc and bcc in the TB-SMA model is not ensured in a general way. In Fig. 1 we display the differences in cohesive energy at $T=0$ K between bcc and hcp (solid line), and between fcc and hcp (dashed line), obtained at constant pressure for different sets of potential parameters corresponding to increasing cutoff radius. The case reported is cobalt, but the same behavior is typical for all the metals we treated in our study. At small values of the cutoff, the bcc structure is preferentially stable (though the equilibrium lattice parameter is twice as large than r_0), whereas at larger cutoff the energies of the hcp and fcc phases become very close to one another, the fcc and hcp structures being alternately stable. For all hcp metals we treated, the stability is better ensured with cutoff values ranging between $\sqrt{11/3}r_0$ and $\sqrt{5}r_0$, that corresponds to including seven or eight shells or neighbors. However, the energy barrier for structural transitions is generally very high, and potentials including any number of neighbor shells greater than five or six can be reasonably used. The fact that a potential based on functionals of central interactions may

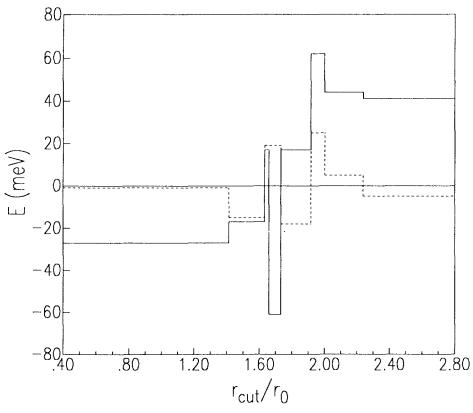

FIG. 1. Cohesive energy differences between bcc and hcp (solid line) and between fcc and hcp (dashed line) structures for cobalt. Data refer to potentials with increasing cutoff ranges. The set of parameters for each potential results from a different fitting run, and cohesive energy is statically minimized with respect to the independent variation of a and c/a ratio.

TABLE III. Parameters of TB potentials for hcp transition metals. First lines contain potential parameters obtained with β equal to the experimental value, second lines (Ti, Zr, and Cd) with variable β in the fitting.

Metal	A (eV)	ξ (eV)	p	q	β
Ti	0.1519	1.8112	8.620	2.390	1.5874
	0.0741	1.4163	11.418	1.643	1.6354
Zr	0.1934	2.2792	8.250	2.249	1.5925
	0.0523	1.4489	13.940	1.071	1.6409
Co	0.0950	1.4880	11.604	2.286	1.6232
Cd	0.1420	0.8117	10.612	5.206	1.8856
	0.0416	0.4720	13.639	3.908	1.6511
Zn	0.1477	0.8900	9.689	4.602	1.8562
Mg	0.0290	0.4992	12.820	2.257	1.6235

TABLE IV. Values of the fitted quantities for hcp transition metals and the simple metal Mg. First lines: results obtained with β equal to the experimental value; (a): results with variable β; (b) experimental values (see Table II); (c) third-neighbor EAM model (Ref. 9).

	$-E_c$	a	C_{11}	C_{12}	C_{13}	C_{33}	C_{44}	$\langle B \rangle$	$\langle G \rangle$
Ti	4.853	2.492	1.473	0.785	0.764	1.980	0.305	1.066	0.368
		(a)	1.796	0.747	0.596	2.178	0.375	1.105	0.531
		(b)	1.761	0.868	0.683	1.891	0.508	1.098	0.504
		(c)	1.835	0.78	0.67	1.992	0.409	1.100	0.505
Zr	6.167	3.232	1.301	0.690	0.657	1.744	0.261	0.936	0.326
		(a)	1.644	0.621	0.473	1.898	0.368	0.958	0.510
		(b)	1.544	0.672	0.646	1.725	0.363	0.971	0.422
		(c)	1.589	0.703	0.61	1.73	0.344	0.973	0.425
Co	4.386	2.507	3.142	1.408	1.223	3.991	0.667	2.039	0.893
		(b)	3.195	1.661	1.021	3.736	0.824	1.948	0.911
Cd	1.166	2.959	0.886	0.834	0.397	0.208	0.005	0.697	0.087
		(a)	0.971	0.492	0.402	0.948	0.157	0.629	0.229
		(b)	1.292	0.400	0.409	0.567	0.242	0.621	0.314
Zn	1.359	2.653	1.177	0.018	0.568	0.404	0.010	0.885	0.119
		(b)	1.791	0.375	0.554	0.688	0.459	0.804	0.625
Mg	1.519	3.176	0.605	0.261	0.223	0.731	0.134	0.381	0.175
		(b)	0.635	0.263	0.216	0.657	0.184	0.369	0.193
		(c)	0.65	0.25	0.202	0.703	0.152	0.368	0.191

succeed in stabilizing noncubic structures should not be surprising, as this is related to the inhomogeneity of functionals containing various functions depending only on a, only on β, and both on a and β, as a function of the cutoff radius. The capability of stabilizing a noncubic structure appears then essentially related to the extension of the interaction to a longer range than first neighbors.

B. bcc structure metals

The equations expressing cohesive energy, equilibrium conditions, and elastic constants for bcc metals are the same for the fcc lattice, with different distances between neighbors and number of neighbors per shell. We have actually tried to fit TB-SMA potential parameters also for bcc metals with some success: for example, in the case of vanandium we obtained a perfectly equilibrated system at $T=0$ K with the correct experimental values of $a_0=3.034$ Å and $E_c=-5.316$ eV, also reproducing the elastic constants with an average discrepancy of 20% and the bulk modulus within 4%, with the following values of the parameters: $A=0.6124$ eV, $\xi=2.441$ eV, $p=5.206$, $q=1.22$. A similar situation was met with molybdenum.

The potential produces a stable bcc configuration for V at $T=0$ K, the energy of any fcc and hcp structure being higher. The lowest-energy differences, obtained by MD relaxation at constant zero pressure and zero temperature, were between the bcc at $a_0=3.034$ Å and a fcc with $a_0=3.877$ Å ($\Delta E=+0.148$ eV), and between the same bcc and an hcp with $a_0=2.774$ Å and $\beta=1.544$ ($\Delta E=+0.069$ eV). However, at any finite temperature the crystal becomes unstable with respect to transition to a fcc structure. The transition proceeds with spontaneous stretching of the system along the bcc [001] direction by a factor of $\sqrt{2}$, the [100] and [010] directions, respectively, transforming into the [110] and [$\bar{1}$10] fcc directions.

Some relevant features of the metallic bonding should make the TB-SMA inadequate in the case of bcc structure. From the electronic point of view, the close-packed structure elements at the extremes of the transition-metal series have an almost empty or almost full d band, whereas in the middle of the series there is a large bonding energy arising from the unbalance between filled bonding states (above the band center) and unfilled antibonding states (below the band center). The cohesive energy is correspondingly larger for bcc structures than for close-packed structures with higher coordination. Concerning elastics properties, it is perhaps relevant that bcc metals have anisotropy ratios generally smaller than unity and the so-called "Cauchy pressure" $P_c=\frac{1}{2}(C_{12}-C_{44})$ is comprised between 0.25 and 0.5 Mbar, whereas close-packed structure transition metals have C/C' always much larger than unity and P_c values typically comprised between 0, and 0.2 Mbar. On this basis, it is felt that the requirements for a bcc transition-metal TB potential are mutually exclusive in our four-parameter scheme (2)–(4).

It has to be recalled, however, that former treatments of bcc transition metals with potentials based on SMA or similar approximation schemes, like FS or EAM, are far from being completely successful: even if a stable body-centered phase is observed, negative values for the thermal expansion[26] and a generally unsatisfactory comparison with phonon dispersion curves[27,28] are found, even if larger sets of free parameters and longer interaction ranges are adopted.[29] As mentioned in Sec. II above, structural stability and elastic properties of non-close-packed structures require a more detailed description of the electron DOS with inclusion of at least five moments

of the distribution.[18,30] Indeed, from the calculated electron DOS (Ref. 31) it is apparent that, whereas close-packed structures have quite flat distributions, bcc structures are in turn characterized by a pronounced dip (the "pseudogap") near the band center, the two branches at the left, and at the right of the band center being asymmetric. In the moments' language, this corresponds to a bimodal behavior which is reflected in the higher-order moments, the asymmetry being related to the odd moments of the distribution, whereas a description limited to μ_2 is equivalent to consider a rectangular approximation for the d-band DOS. This latter is evidently adequate for close-packed structures, whereas it is completely unreliable for treating bcc structures.

C. fcc-based alloys

Several binary intermetallic compounds of technological interest crystallize in the cubic structures $L1_0$ and $L1_1$ (AB-type alloys), and $L1_2$ (A_3B-type alloys). These structures are fcc-based, the first two being fcc crystals with alternating A and B layers in the (002) and (222) planes, respectively, and the latter being a fcc crystal with atoms A placed on the faces and atoms B on the corners of the basic cube. Other structures, only slightly more exotic, may be classified under the category of fcc-based phases, as for example, $D0_{22}$ and the so called "$MoPt_2$." Such structures have a bcc basic cell resulting by multiplicating the period of the underlying fcc lattice along the [010] and the [110] directions, respectively, and give rise to ordered systems with A_3B and A_2B stoichiometry. With the exception of $L1_2$, whose cell is simple cubic, all the above structures can exhibit tetragonal ($L1_0$ and $D0_{22}$), orthorhombic ($MoPt_2$), and rhombohedral ($L1_1$) distorsions.

Cubic alloys have been formerly modeled in terms of pair potentials, to study planar faults in A_3B compounds as a function of the heat of mixing;[32] more recently, the EAM model has been used to predict the surface segregation properties for some AB compounds (single impurities in host metal matrices),[6] and to model elastic and defect properties of bulk Ni_3Al.[33] The potentials for binary intermetallic alloys with fcc-based structure are easily derived in the TB-SMA model, starting from the potentials already calculated for the pure elements and under the further assumption that the A-A and B-B interactions in the compound system are the same as in the respective pure systems. The cohesive energy equation is recasted in the form

$$E_c = wE_c^A + (1-w)E_c^B + \Delta H_{\text{mix}} \tag{6}$$

with $w=\frac{1}{2}$ for AB, $\frac{2}{3}$ for A_2B, and $\frac{3}{4}$ for A_3B alloys, E_c^α the cohesive energy of pure α, and ΔH_{mix} the alloy's experimental heat of mixing at that particular stoichiometry. Then, the eight interaction parameters for the like atoms being fixed, only the four cross-interaction parameters A_{AB}, ξ_{AB}, p_{AB}, and q_{AB} are left free for the minimization.

We summarize the results obtained for two alloys Cu_3Au and Ni_3Al, both with $L1_2$ structure. The potential parameters are reported in Table V, and the quantities resulting from the fitting procedure in Table VI. In both cases, the reproduction of the $T=0$ K fitted data is again very good. The TB second-moment potential hereby derived is able to predict with surprising precision the occurrence of the structural order-disorder transition in Cu_3Au,[34] also elucidating some interesting features of the phenomenon, like the persistence of short-range order above T_c, and the role of vibrational entropy, derived from the phonon spectra in the quasiharmonic approximation, in determining the first-order character of the transition. Also the structural changes occurring in Ni_3Al upon introduction of chemical disorder have been successfully reproduced.[35]

TABLE V. TB potential parameters for the $L1_2$ alloys Cu_3Au and Ni_3Al.

	A (eV)	ξ (eV)	p	q
Cu_3Au	0.1539	1.5605	11.05	3.0475
Ni_3Al	0.0563	1.2349	14.997	1.2823

IV. VERIFICATION OF THE LONG-RANGE TB-SMA POTENTIALS ON EXPERIMENTAL DATA

A. Static properties

All the experimental values for point-defect properties reported in this subsection have been taken from the review paper by Wollenberger.[36] In particular, vacancy enthalpy of formation $\Delta H^{f,v}$ and volume of formation $\Delta V^{f,v}$, interstitial volume of formation $\Delta V^{f,i}$ (either self-interstitial or Frenkel pairs), and formation enthalpy $\Delta H^{f,v}$. To estimate these quantities we have adopted a quasidynamical relaxation procedure, in order to minimize the local strain related to the abrupt insertion, or removal, of an atom from an equilibrated system. A MD simulation at a very low temperature (of the order of 0.1 K) is carried out on a system made up of 256 atoms arranged in the fcc structure, or 250 atoms arranged in the hcp structure, and an atom is added at, or removed from, a lattice site by progressively "inflating," or "deflating," it. Such a procedure is performed by scaling the components of the energy and of the force constants relative to that atom by a factor proportional to the logarithm of the simulation time. When the atom has fully appeared, or disappeared, the system continues to relax at the same low temperature for some time, before being definitely quenched down to $T=0$ K, with a steepest-descent gra-

TABLE VI. Values of the fitted quantities for the $L1_2$ alloys Cu_3Au and Ni_3Al. First lines, calculated data; second lines, experimental data from Kittel and Simmons-Wang (see Table II).

	$-E_c$	a_0	C_{11}	C_{12}	C_{44}	$\langle B \rangle$	C'
Cu_3Au	3.545	3.615	1.92	1.37	0.80	1.55	0.27
	3.545	3.615	1.89	1.32	0.74	1.51	0.28
Ni_3Al	4.54	3.567	2.43	1.48	1.26	1.79	0.48
	4.54	3.567	2.30	1.50	1.31	1.77	0.40

dient search technique.[37] We then estimate the enthalpy of formation of a defect by comparing the energy of the as-obtained defective system to the energy of the perfect system with N-1 atoms, the formation enthalpy at $P=0$ and $T=0$ K being equal to the formation energy $\Delta E^{f,v}$; the formation volume is, in turn, obtained by direct comparison of the total system volumes.

The values of different point-defect properties calculated with the potentials of the present work are reported in Table VII for some fcc (Cu, Ni, Au, Ag, Pt) and hcp metals (Zr and Co), and are compared to existing experimental data and to former evaluations, also reported by Wollenberger. The comparison appears quite satisfactory. In particular, we note that the empirical $\frac{1}{3}$ value for the ratio $\Delta E^{f,v}/E_c$ naturally results from the model, whereas in the EAM the experimental value of $\Delta E^{f,v}$ is usually imposed during the fitting procedure. For fcc metals the ⟨100⟩ dumbbell configuration results to be always the most stable self-interstitial position; though experimental measurements are scarce, due to the difficulty to resolve self-interstitial symmetry, this evidence is safely established at least in Cu and Ni.

Phonon dispersion curves were obtained by expressing the model force constants in the quasiharmonic approximation.[38] The dispersion curves for fcc copper at $T=80$ K and for hcp cobalt at room temperature are shown in Figs. 2 and 3, respectively, together with experimental results.[39,40] The agreement for Cu is again very good, apart from a 5% discrepancy around the X point. More generally, this slight disagreement is evident for the whole paths, like X-W-X, in the vicinity of the Brillouin zone borders. Similarly, a quite good agreement is obtained for Co. The strong softening of the LO mode around the Γ point, common to several hcp metals, has been recognized[41] to be due to peculiarities in the electronic structure around the Fermi level that cannot be reproduced by the simple model of electron DOS common to TB, EAM, and FS empirical potentials.

TABLE VII. Miscellaneous $T=0$ K enthalpies and volumes of formation of point defects for some fcc and hcp metals calculated with the potentials of the present work. Experimental data in parentheses are from Wollenberger (Ref. 36) (underscored data are estimated from first-principles calculations).

	Point defect	ΔH^f (eV)	ΔV^f (a.u.)
Cu	Vacancy	1.25(1.0–1.3)	−0.89(−0.8)
	⟨100⟩ split	3.19(2.2–5.8)	1.15(1.1–1.5)
	⟨110⟩ split	3.28(−)	0.91(−)
	⟨111⟩ split	3.21(3.8–4.3)	1.48(1.4–1.6)
	Octahedral	3.30(2.4–6.1)	1.27(1.2–2.0)
	Tetrahedral	3.76(3.7–3.9)	1.34(1.4–1.5)
	Average	3.35(1.7–4.3)	1.23(1.3–1.7)
	Frenkel	4.45(2.9–5.5)	1.96(−)
Ni	Vacancy	1.95(1.5–1.7)	−0.85(−0.78)
	⟨100⟩ split	5.26(4.08)	1.96(1.7)
	⟨100⟩ split	5.50(−)	1.11(−)
	⟨111⟩ split	5.31(4.24)	2.14(−)
	Octahedral	5.28(−)	1.88(−)
	Tetrahedral	6.64(−)	2.42(−)
	Average	5.60(−)	1.90(1.8)
Ag	Vacancy	0.88(1.1–1.2)	−0.85(−)
Pt	Vacancy	1.17(1.2–1.5)	−0.73(−0.6–0.7)
Au	Vacancy	0.75(0.9–1.0)	−0.63(−0.5–−0.8)
Zr	Vacancy	2.21(>1.55)	−0.74
Co	Vacancy	1.56(1.38)	−0.24(−)

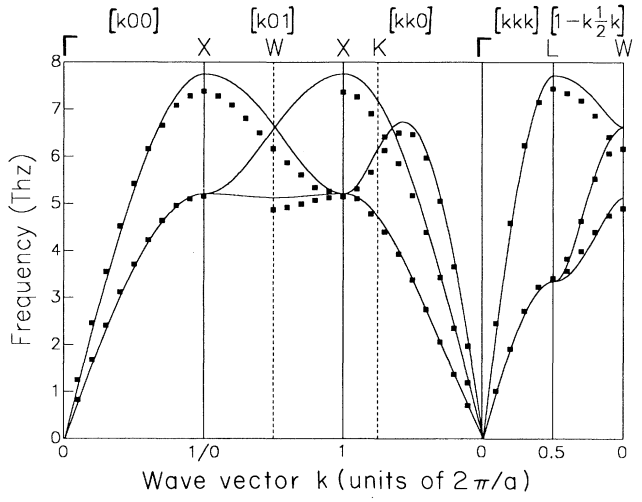

FIG. 2. Phonon dispersion curves for fcc copper at 80 K along the higher symmetry directions. Experimental points from Nilsson and Rolandson (Ref. 39).

In Table VIII we report a comparison between the calculated and experimental values of the frequencies ν_X and ν_L at the bordering points X and L of the first Brillouin zone for the transverse (T) and longitudinal (L) branches, for some fcc metals. The agreement is good for Cu and Ag, the error being of few percents, and acceptable for Ni, Pd, and Pt, for which the predicted values lie within 5–15 % from the experimental ones. This has to be considered as a severe test for the model, in that it explores the capability of long-range potentials of reproduc-

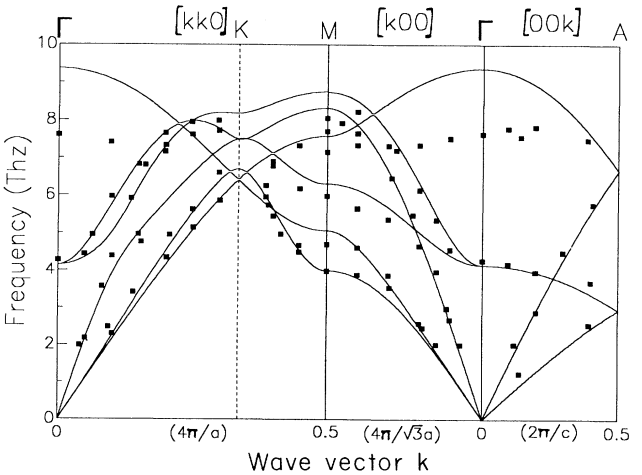

FIG. 3. Phonon dispersion curves for hcp cobalt at room temperature along the higher symmetry directions. Experimental points from Wakabayashi *et al.* (Ref. 40).

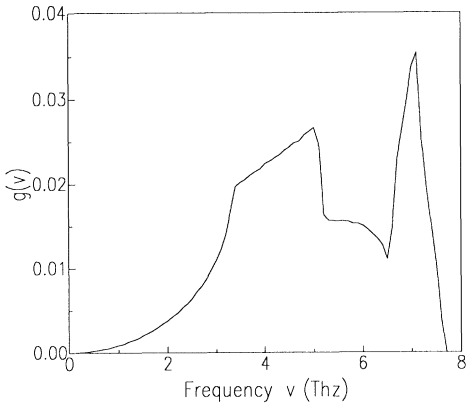

FIG. 4. Phonon density of states for fcc copper at 80 K.

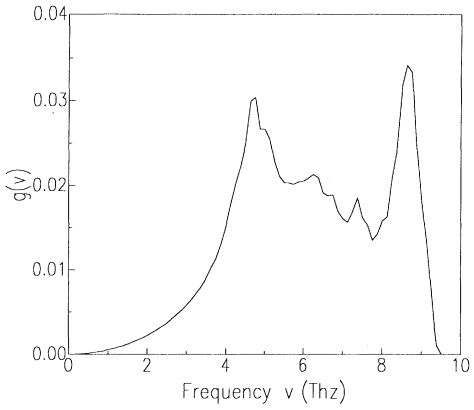

FIG. 5. Phonon density of states for hcp cobalt at room temperature.

ing both elastic properties at the center (the elastic constants) and at the borders of the Brillouin zone, without having been explicitly fitted on the phonon dispersion curves. The case of Au, for which the disagreement is particularly evident, deserves, however, some comments. It has been noted experimentally[41] that Au has a different elastic behavior at finite temperatures from the other noble metals Cu and Ag. This is generally ascribed to a strong contribution from noncentral many-body forces, that appear to be of increasing importance along the noble metal series. As we adopt a spherically symmetric model, without particular prescriptions for angular forces, the larger error in elastic properties of Au should not be surprising.

In the same quasiharmonic approximation, the phonon frequency spectra have been computed; examples for fcc copper and hcp cobalt are shown in Figs. 4 and 5. Phonon dispersion curves and frequency spectra for ordered and disordered Cu_3Au have been reported elsewhere.[43] In Figs. 6 and 7, $\omega(k)$ and $g(\omega)$ for Ni_3Al are displayed; we note that these results are in striking agreement with those obtained by Foiles and Daw[33] with an EAM potential, this latter giving a 3% smaller cutoff frequency than the TB result.

B. Finite-temperature properties

All the following calculations of thermodynamic properties of metals at finite temperatures were obtained by MD simulations in the canonical ensemble (NVT) or in the NPT isoenthalpic-isobaric ensemble, with the Nosé-Andersen technique.[44–46] The equations on motion for systems of 500 particles for cubic structures, and of 432 particles for hexagonal systems (corresponding to $5\times5\times5$ and $6\times6\times6$ basic cells, respectively) are integrated using a fifth-order Gear predictor-corrector algorithm[47] with a time step of 10^{-15} s, and imposing usual toroidal boundary conditions. An example of the temperature behavior of system enthalpy and volume is reported in Fig. 8 for Cu_3Au; the two discontinuities in the

TABLE VIII. Comparison between calculated and experimental longitudinal (L) and transverse (T) phonon frequencies at the Brillouin zone boundaries X and L for some fcc metals. First lines, calculated data; second lines experimental data [Cu at 80 K (Ref. 39), Ag (Ref. 41), Au (Ref. 42), Ni (Ref. 62), and Pd (Ref. 63) at room temperature, and Pt at 90 K (Ref. 64)]. Frequencies are expressed in Thz.

	$\nu_X(L)$	$\nu_X(T)$	$\nu_L(L)$	$\nu_L(T)$
Cu	7.75	5.21	7.71	3.34
	7.38	5.16	7.44	3.41
Ag	4.80	3.31	4.75	2.17
	4.96	3.37	5.13	2.27
Au	3.20	1.51	3.24	2.27
	4.61	2.75	4.70	1.86
Ni	9.88	6.78	9.80	4.49
	8.51	6.21	8.84	4.26
Pd	5.77	4.02	5.72	2.67
	6.72	4.64	7.02	3.34
Pt	4.95	3.94	4.87	2.25
	5.80	3.84	5.85	2.90

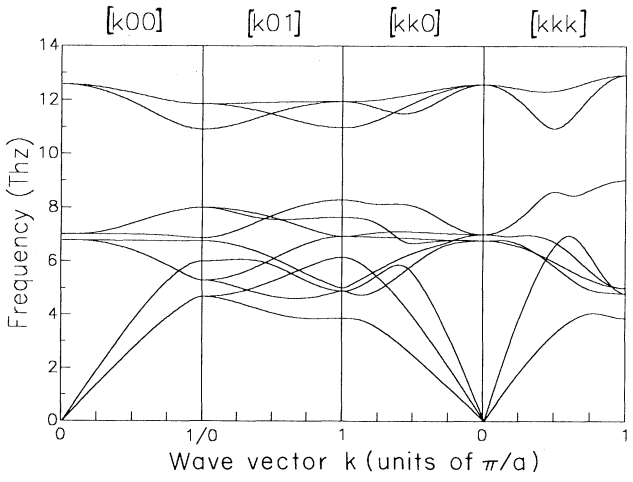

FIG. 6. Phonon dispersion curves for $L1_2$ Ni_3Al at 0 K along the higher symmetry directions of the simple-cubic lattice.

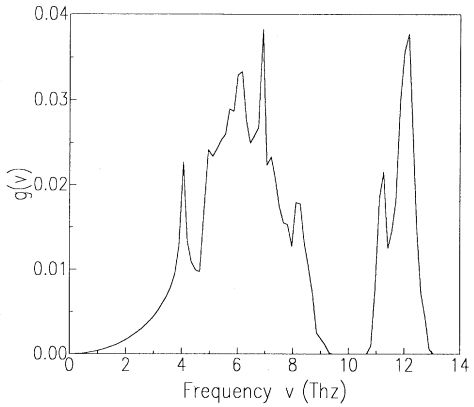

FIG. 7. Phonon density of states for $L1_2$ Ni_3Al at 0 K.

plots correspond to the disordering transition at $T_c = 635$ K and to melting at $T_m = 1420$ K. The results obtained for various thermal properties of the fcc metals Ni, Ag, and Cu, for hcp Co and for the $L1_2$ alloy Cu_3Au are reported in Table IX.

From the low-temperature behavior of the system enthalpy, the value of the constant-pressure specific heat can be deduced by drawing a curve for $c_p(T_i)$. The linear coefficients of the best fit to these curves are reported in Table IX, and compare quite well with the experimental values[48] for Ni and Ag, whereas for Cu and hcp Co it lies within about 20%.

Correspondingly, from the low-temperature behavior of the system volume we deduce the thermal expansion coefficient and we compare the linear coefficient of the best fit to the curve $\alpha = \alpha(T_i)$ with the experimental values of linear thermal expansion.[49] In most cases we find a reasonable agreement with experimental data, the errors being within 10–15%, though all the results but Ni tend to be overestimated.

From the height of the jumps in the system enthalpy and volume, the latent heat and volume of melting ΔH_m and ΔV_m can be estimated. All the results, reported in Table IX, compare very well with the experimental data,[48] the errors being within a few percent, with the only exception of the ΔV_m value for Ag, which is overestimated by about 40%. Comparison of the equation of state at finite temperatures with experimental results requires the vibrational free-energy contribution to be added to the zero-temperature term, simply related to the static properties of the model. This vibrational contribution can be shown to be related to the thermal Grüneisen constant γ_{th},[50] under the hypothesis that all the constants γ_i for each eigenfrequency ω_i of the system are equal. The constant γ_{th} can then be defined

$$\gamma_{\text{th}} = \frac{3B\alpha V}{c_v} . \tag{7}$$

Inserting in the above equation the calculated values of lattice thermal expansion α, average bulk modulus B, and atomic volume V, and taking $c_v \cong 3Nk_B$ at room temperature for the systems considered, the corresponding values of the thermal Grüneisen constant can be calculated from our model. Except for Ni, the resulting values are more or less overestimated, and this fact, coupled to the tendency to slightly overestimate the thermal expansion coefficients, indicates a too large anharmonicity of the TB potentials.

The melting temperature in Table IX is identified by monitoring the jump in the system enthalpy and volume, and the vanishing of the structure factor $S(\mathbf{k})$ defined as

$$S(\mathbf{k}) = \frac{1}{N} \sum_{i \neq j} e^{i\mathbf{k}\cdot(r_i - r_j)} \tag{8}$$

for some $\mathbf{k} = (k_x, k_y, k_z)$ in the reciprocal space. The results obtained for the various model systems are rather satisfactory, when considering that they correspond to perfect infinite systems that are driven to melting without any vacancy buildup. The slight overestimate (around 10%) of $T_m s'$ is thus not surprising being, in turn, an indirect confirmation of the reliability of the potential model. A remarkable exception to this trend is Au, for which the melting point is considerably underestimated by the TB potential. This has to be coupled with the previous observation of a calculated phonon cutoff frequency much lower than the experimental one (see Table VIII),

TABLE IX. Miscellaneous finite-temperature properties for Ni, Ag, Cu, Co, and Cu_3Au calculated with the potentials of the present work: melting temperature T_m (K), latent heat of fusion ΔH_m (Kcal/mol), latent volume of fusion ΔV_m (a.u.), constant-pressure specific heat C_p (cal/K/mol) and linear expansion coefficient α (10^{-5} K^{-1}) between 0 and 600 K, thermal Grüneisen constant γ_{th}, enthalpy of the liquid at the melting point H_m^l minus the STP value H_0 (Kcal/mol), density of the liquid at the melting point ρ_m^l (g/cm^3). Experimental data in parentheses are taken from the compilation by Hultgren *et al.* (Ref. 48).

	Ni	Ag	Cu	Co	Cu_3Au
T_m	1880(1726)	1330(1234)	1490(1356)	1950(1768)	1420(1233)
ΔH_m	4.08(4.17)	2.77(2.70)	3.07(3.11)	3.52(3.87)	2.08(2.76)
ΔV_m	1.14(1.07)	1.46(1.03)	0.86(0.84)	0.70(0.85)	0.91(−)
C_p	8.71(8.60)	7.05(6.87)	8.30(6.59)	7.87(6.52)	5.94(5.89)
α	1.42(1.50)	2.47(2.14)	2.10(1.83)	1.71(1.38)	5.43(4.89)
γ_{th}	1.92(1.90)	2.96(2.40)	2.30(1.96)	2.51(1.94)	
$H_m^l - H_0$	17.3(15.4)	9.45(8.99)	14.4(10.1)	14.8(16.8)	8.13(−)
ρ_m^l	6.86(7.84)	8.60(9.34)	7.09(7.98)	7.49(7.67)	11.11(−)

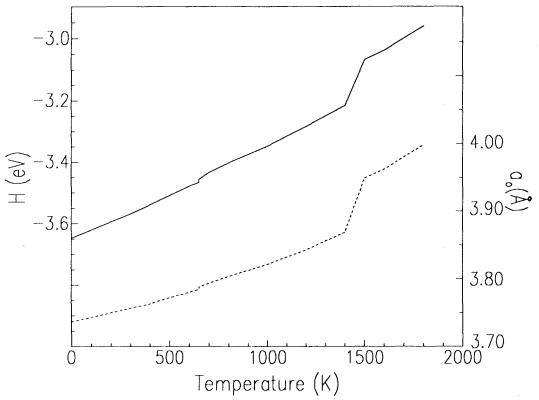

FIG. 8. Temperature behavior of system enthalpy (solid curve, left scale in eV) and lattice parameter (dashed curve, right scale in Å) for Cu_3Au. The structure is ordered $L1_2$ below $T_c = 635$ K, disordered $A1$ between T_c and $T_m = 1420$ K.

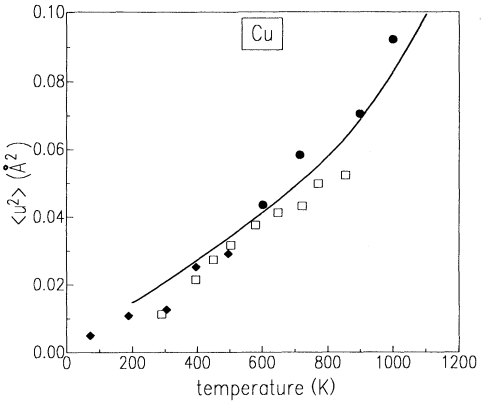

FIG. 10. Atomic MSD curve for fcc copper. Experimental points: □, from Owen and Williams (Ref. 55), ♦, from Flinn *et al.* (Ref. 56), ●, from Martin and O'Connor (Ref. 57).

which is a clear signature of a too large lattice dilation at high temperatures, and results in an anticipated melting of the model system. The location of the melting temperature undoubtedly is among the quantities that appear to be most sensible to the range of the interaction. This point will be discussed in more detail below.

From the absolute values of system enthalpy and volume immediately above the melting point, an estimate can be given for the enthalpy and density of the liquid at melting. The results, presented in Table IX as well, are in rather good agreement with the experimental data.[48]

Atomic mean-square displacement (MSD) is among the most difficult finite-temperature quantities to compare with experimental data. As for the location of melting temperatures, this is not only related to the intrinsic excess of anharmonicity that can affect many-body potentials, but also to the fact that a too short cutoff of the interaction entails a technical difficulty in MD simulations. In fact, with increasing temperature and lattice dilation, some particles can "escape" such a short cutoff, so that the average coordination in the system is strongly reduced. This implies that each atom experiences a drastically reduced restoring force and then the MSD tends to be more and more amplified. Indeed, following Lindemann's law[51,52] the melting point can be empirically related to the temperature dependence of MSD, so that this also explains why a short-range cutoff always leads to anticipated melting. In our calculations, MSD are directly estimated by recording the displacements of the particles from their equilibrium position and averaging the square of this quantity over a sufficiently long equilibrium trajectory. In Figs. 9–11 we compare our calculated MSD's (solid curves) with experimental data for Ni,[53,54] Cu,[55–57] and Ag.[58,59] It is evident that, as for the melting temperature T_m, extension of the interaction to long range as the fifth-neighbor distance is successful in removing both the problems of excessive anharmonicity and the technical limitation of particle escape. The residual anharmonicity that manifests in the errors on the Grüneisen constants is not eliminable by a simple extension of the potential cutoff, but appears to be inherent to the model.

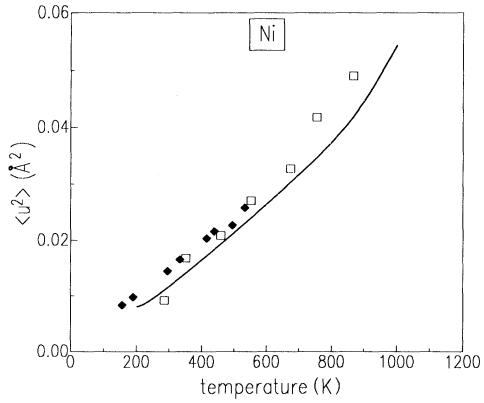

FIG. 9. Atomic MSD curve for fcc nickel. Experimental points: □, from Simerska (Ref. 53), ♦, from Wilson *et al.* (Ref. 54).

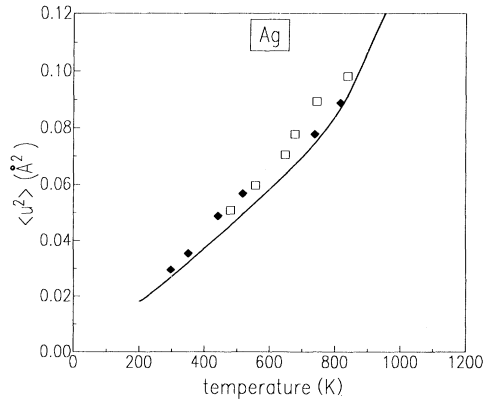

FIG. 11. Atomic MSD curve for fcc silver. Experimental points: □, from Haworth (Ref. 58), ♦, from Simerska (Ref. 59).

V. CONCLUSIONS AND COMMENTS

We have presented a family of many-body potentials for fcc and hcp transition metals and fcc-based alloys, developed on the basis of a second-moment approximation of the tight-binding, or linear combination of atomic orbitals (LCAO), scheme employed by Tomànek, Aligia, and Balseiro.[15] This is a very "chemical" point of view, as it is related in a natural way to the metallic character of the cohesive energy. The range of the interaction has been extended up to the fifth-neighbor shell. The potential parameters have been adjusted so as to reproduce cohesive energy, atomic volume, and elastic constants of the corresponding real systems at $T=0$ K, though ensuring stability of the appropriate crystal structure. These potentials have proved to satisfactorily reproduce experimental quantities, like formation energies and formation volumes of simple point defects as vacancy, self-interstitials of different types (tetrahedral, octahedral, dumbbell along various directions), and dissociated Frenkel pair. Concerning lattice dynamical properties, it is worth noting that calculated phonon dispersion curves compare well with experimental measurements for both fcc and hcp metals and, in particular, the frequencies at the edge of the Brillouin zone are reproduced in most cases.

Extension of the interaction to a longer range as the fifth-neighbor distance has been attempted in order to reproduce high-temperature properties of real systems that are usually beyond the capability of short-range potentials. Indeed, this extended potential scheme gives correct estimates for various thermodynamic quantities up to the melting point, like specific heat, average linear thermal expansion coefficient, thermal Grüneisen constant, latent heat, and volume of melting, enthalpy, and density of the liquid at the melting point. The temperature behavior of the mean-square displacements is also quite accurately reproduced. This fact is reflected in the rather good agreement between calculated and experimental melting temperatures which, as for the mean-square displacements, usually frustrates any effort of quantitative reproduction.

We have often recalled, throughout this paper, that the second-moment, or μ_2, approximation to the electron density of states suffers intrinsic limitations that make it unsuitable to describe (a) the relative stability of the face-centered, hexagonal, and body-centered structures along the transition series, (b) the possibility of obtaining β ratios for hexagonal crystals different from the "ideal" value of $\sqrt{8/3}$, (c) the reconstruction of some surfaces, especially in the case of bcc crystals, and (d) the physical properties of noble metals Cu, Au, and Au. Nevertheless, apart from point (c), that was not treated in the present work, we have shown that with long-ranged μ_2 approximation, point (d) is well resolved, except for some features of Au, point (b) can be solved at least in those cases having "nonpathological" values of β, and point (a) can be reasonably demonstrated, at least for the relative stability of close-packed structures, with a suitable choice of the cutoff length of the interactions. This implies that metals like Cd or Zn are not suitable for a TB treatment of the type displayed here. We stress that, in particular, for points (a) and (b), the success of the model is essentially due to the extension of the range of the interaction beyond first-neighbor distance. If we disregard the possibility of a fortuitous agreement, we can argue that the hopping integrals being defined between first-neighboring atoms, the extension to nextcoming shells of neighbors should begin to collect in the effective interaction some contributions from the moments of higher order.

[1] M. S. Daw and M. I. Baskes, Phys. Rev. Lett. **50**, 1285 (1983); Phys. Rev. B **29**, 6443 (1984).
[2] M. W. Finnis and J. F. Sinclair, Philos. Mag. A **50**, 45 (1984).
[3] V. Rosato, M. Guillope, and B. Legrand, Philos. Mag. A **59**, 321 (1989).
[4] R. Car and M. Parrinello, Phys. Rev. Lett. **55**, 2471 (1985).
[5] C. Massobrio, V. Pontikis, and G. Martin, Phys. Rev. Lett. **62**, 1142 (1989).
[6] S. M. Foiles, M. I. Baskes, and M. S. Daw, Phys. Rev. B **33**, 7983 (1986).
[7] A. P. Sutton and J. Chen, Philos. Mag. Lett. **61**, 139 (1990).
[8] M. J. Sabochick and N. Q. Lam, Phys. Rev. B **43**, 5243 (1991).
[9] D. Wolf, P. R. Okamoto, S. Yip, J. F. Lutsko, and M. Kluge, J. Mater. Res. **5**, 286 (1990).
[10] D. J. Oh and R. A. Johnson, J. Mater. Res. **3**, 471 (1988).
[11] G. J. Ackland and R. Thetford, Philos. Mag. A **56**, 15 (1987).
[12] F. Ducastelle, in *Computer Simulation in Materials Science*, Vol. 205 of NATO Advanced Study Institute, Series E, Appl. Phys., edited by M. Meyer and V. Pontikis (Kluwer, Dordrecht, 1991).
[13] A. P. Sutton, M. W. Finnis, D. G. Pettifor, and Y. Ohta, J. Phys. C **21**, 35 (1988).
[14] D. J. Chadi, Phys. Rev. B **19**, 2074 (1979).
[15] R. P. Gupta, Phys. Rev. B **23**, 6265 (1985), and references therein; D. Tomànek, A. A. Aligia, and C. A. Balseiro, *ibid.* **32**, 5051 (1985).
[16] B. Loisel, D. Gorse, V. Pontikis, and J. Lapujoulade, Surf. Sci. **221**, 365 (1989).
[17] F. Willaime and C. Massobrio, Phys. Rev. Lett. **63**, 2244 (1989).
[18] F. Ducastelle, J. Phys. (Paris) **31**, 1055 (1970).
[19] G. Allan and M. Lannoo, Surf. Sci. **89**, 142 (1979).
[20] J. C. Slater and G. F. Koster, Phys. Rev. **94**, 1498 (1954).
[21] P. Turchi and F. Ducastelle, in *The Recursion Method and Its Applications*, edited by D. G. Pettifor and D. L. Weaire (Springer-Verlag, Berlin, 1985).
[22] M. W. Finnis, A. T. Paxton, D. G. Pettifor, A. P. Sutton, and Y. Ohta, Philos. Mag. A **58**, 143 (1988).
[23] K. W. Jacobsen, J. K. Nørskov, and M. J. Puska, Phys. Rev. B **35**, 7423 (1987).
[24] M. S. Daw, Phys. Rev. B **39**, 7441 (1989).
[25] K. Maeda, V. Vitek, and A. P. Sutton, Acta Metall. **30**, 2001 (1982).
[26] M. Marchese, G. Jacucci, and C. P. Flynn, Philos. Mag. Lett. **57**, 25 (1988).
[27] R. Rebonato and J. Q. Broughton, Philos. Mag. Lett. **55**, 225

(1987).
[28]J. Eridon and S. Rao, Philos. Mag. Lett. **59**, 31 (1989).
[29]J. B. Adams and S. M. Foiles, Phys. Rev. B **41**, 3316 (1990).
[30]F. Ducastelle, *Order and Phase Stability in Alloys* (North-Holland, Amsterdam, 1991), Sec. 6.
[31]O. K. Andersen, J. Madsen, U. K. Poulsen, O. Jepsen, and J. Kollar, Physica B **86-88**, 249 (1977).
[32]M. Yamaguchi, V. Vitek, and D. P. Pope, Philos. Mag. A **43**, 1027 (1981).
[33]S. M. Foiles and M. S. Daw, J. Mater. Res. **2**, 5 (1987).
[34]F. Cleri, G. Mazzone, and V. Rosato, Phys. Rev. B (to be published).
[35]F. Cardellini, F. Cleri, G. Mazzone, A. Montone, and V. Rosato, J. Mater. Res. (to be published).
[36]H. J. Wollenberger, in *Physical Metallurgy,* 3rd ed., edited by R. W. Cahn and P. Haasen (Elsevier, Amsterdam, 1983).
[37]R. Beeler and G. L. Kulcinski, in *Interatomic Potentials and Simulation of Lattice Defects,* edited by P. C. Gehlen, J. R. Beeler, and R. I. Jaffee (Academic, New York, 1975), p. 85.
[38]A. A. Maradudin, E. W. Montroll, G. H. Weiss, and I. P. Ipatova, *Solid State Physics Suppl. 3,* 2nd ed. (Academic, New York, 1972).
[39]G. Nilsson and S. Rolandson, Phys. Rev. B **7**, 2393 (1973).
[40]N. Wakabayashi, R. H. Scherm, and H. G. Smith, Phys. Rev. B **25**, 5122 (1982).
[41]W. A. Kamitakahara and B. N. Brockhouse, Phys. Lett. **28A**, 639 (1969).
[42]J. W. Lynn, H. G. Smith, and R. M. Nicklow, Phys. Rev. B **8**, 3493 (1973).
[43]F. Cleri and V. Rosato, Philos. Mag. Lett. (to be published).
[44]H. C. Andersen, J. Chem. Phys. **72**, 2384 (1980).
[45]M. Parrinello and A. Rahman, J. Appl. Phys. **52**, 7182 (1981).
[46]S. I. Nosé, J. Chem. Phys. **81**, 511 (1984).
[47]A. Nordsieck, Math. Comput. **16**, 22 (1962).
[48]R. Hultgren, P. D. Desai, D. T. Hawkins, M. Gleiser, and K. K. Kelley, *Selected Values of the Thermodynamic Properties of Binary Alloys* (American Society for Metals, Metals Park, 1973).
[49]W. B. Pearson, *A Handbook of Lattice Spacings and Structures of Metals and Alloys* (Pergamon, London, 1958).
[50]J. C. Slater, *Introduction to Chemical Physics* (McGraw-Hill, New York, 1939), Sec. 13.
[51]F. A. Lindemann, Phys. Z. **11**, 609 (1910).
[52]J. J. Gilvarry, Phys. Rev. **102**, 308 (1956).
[53]M. Simerska, Czech. J. Phys. B **12**, 858 (1962).
[54]R. H. Wilson, E. F. Skelton, and J. L. Katz, Acta Crystallogr. **21**, 635 (1966).
[55]E. A. Owen and R. W. Williams, Proc. R. Soc. London, Ser. A **188**, 509 (1947).
[56]P. A. Flinn, G. M. McManus, and J. A. Rayne, Phys. Rev. **123**, 909 (1961).
[57]C. J. Martin and D. A. O'Connor, J. Phys. C **10**, 3521 (1977).
[58]C. W. Haworth, Philos. Mag. **5**, 1229 (1960).
[59]M. Simerska, Acta Crystallogr. **14**, 1259 (1961).
[60]C. Kittel, *Introduction to Solid State Physics* (Wiley, New York, 1966).
[61]G. Simmons and H. Wang, *Single Crystal Elastic Constants and Calculated Aggregated Properties* (MIT Press, Cambridge, 1971).
[62]R. J. Birgenau, J. Cordes, G. Doling, and A. D. B. Woods, Phys. Rev. **136**, 1359 (1964).
[63]A. P. Muller and B. N. Brockhouse, Can. J. Phys. **49**, 704 (1971).
[64]D. H. Dutton, B. N. Brockhouse, and A. P. Muller, Can. J. Phys. **50**, 2915 (1972).